Thermal aging kinetic and effects on mechanical behavior of fully recycled composite based on polypropylene/polyethylene blend

S. Tamboura,[1] H. Meftah [ID],[1,2] J. Fitoussi,[2] H. BenDaly,[1] A. Tcharkhtchi[2]

[1]LMS, ENISo, Université de Sousse, BP 264 Cité Erriadh, Sousse 4023, Tunisie
[2]Laboratoire PIMM, UMR 8006 CNRS, Arts et Métiers Paris-Tech, Paris 75013, France
Correspondence to: H. Meftah (E-mail: mefteh.hassen988@gmail.com)

ABSTRACT: The effect of thermal oxidation of a fully recycled carbon fibers reinforced stabilized polypropylene/polyethylene blend on the mechanical properties has been studied at 120, 130 and 140 °C. In a first step, several analyses by FTIR and UV spectrometry and differential scanning calorimetry were performed in order to detect and monitor the evolution of the antioxidants and oxidation products in the materials. This approach aims to well understand and identify the aging mechanisms that will be modeled in a second step in a kinetic model capable of predicting the evolution of carbonyl build-up while taking into account the presence of the different antioxidants. Modeling results showed a good correlation between the kinetic behavior and the obtained experimental data. Furthermore, the effect of thermal aging on the mechanical behaviors of the composite and the matrix were studied at the macroscopic scale at different strain rates. It has been shown that the thermal oxidation affects only the elongation at break. The numerical values of the oxidation products generated by the kinetic model allowed linking the evolution of the mechanical behavior under aging with the physicochemical state of the material.

INTRODUCTION

The worldwide use of composite materials in several applications has shown an exponential increase during the past decades thanks to their lightness and mechanical performance.[1] In consequence, wastes from manufacturing and end-of-life products increased as well. Therefore, environmental awareness has increased and led to new global agreements to use more and more recyclable material.[2]

Because of their complex compositions (fibers, matrix, and fillers), it is difficult to completely recycle the composites. For this reason, in the majority of the cases only fibers can be reclaimed using several techniques. Among them is the pyrolysis which is the most widespread used technic to recover fibers.[2,3] In fact, after pyrolysis, the recycled carbon fibers keep more than 90% of their mechanical properties.[4,5] Furthermore, the recycling of polymers has developed during the last two decades. New chemical techniques allow to recycle polymers and reused them as raw materials for new polymer using suitable chemical solvents.[6]

The current study focus on a recycled stabilized blend (polypropylene/polyethylene) reinforced up to 20% wt with recycled short carbon fibers obtained by pyrolysis and milled in order to get an average length of 180 µm. The proposed polymer contains two kinds of stabilizers: one is a phenolic and the second is an organic phosphites. The elaborated composite is intended for automotive applications to absorb higher crashworthiness in a harsh environment (near to the engine where the temperature is relatively high). Thus the composite is subjected to physical and chemical aging condition which may degrade the material during its life time and alter the mechanical performance of the part. Therefore, automakers must take into account the parallel effect of chemical ageing (e.g., oxidation) and mechanical ageing (for example fatigue) on applied performance (e.g., crashworthiness application). In fact, the mechanical behavior of an aged bumper for example during an accident is different from the virgin one. So, in order to increase time to embrittlement and so improve the mechanical properties, agents and stabilizer are added to polymers during extrusion or injection molding.

To characterize the phenomena involved in stabilizer disappearance, a good understanding of its physico-chemistry is required. In fact, this latter can be consumed not only by chemical reactions but also lost by extraction or evaporation and many researches have been realized studying its effect on polymers ageing in terms of its induction period and its consumption rate.[7–9] In order to be able to detect antioxidants, follow their

disappearance and carbonyls build up, many analytical methods are proposed in literature such as IR and UV spectrophotometry and differential scanning calorimetry (DSC) under oxygen (OIT).[10–14] Coupling the chemical consumption and physical loss of stabilizers and proposing valid kinetic models is a complex and interesting field that's why in recent years many researchers have been attracted to study it.[15,16]

This work aims to study in one hand, the thermal aging of the two materials mentioned above, characterize the stabilizer influence on the induction period and propose a kinetic model capable of predicting the consumption of the antioxidants, the induction time and the carbonyl build-up evolution. The mechanistic scheme involving stabilizer used in the current work was used in previous work and some assumptions have been made to simplify the mechanism and the modeling.[17–19] In the other hand, the effect of oxidation on the mechanical behavior is studied in order to link the thermal aging influence on the embrittlement of the composite and the matrix in the quasi-static and dynamic loading.

EXPERIMENTAL

Materials

In this work, two materials are proposed. The first is a 100% recycled polypropylene/polyethylene blend matrix (RPP) designed for crashworthiness in automotive applications. A phenolic antioxidant and an organic phosphites, more precisely the tri (alkylaryl) phosphites, have been added to the matrix during elaboration process in order to better withstand environmental temperatures and delay oxidation. For confidential reasons, the exact structure and formula of the stabilizers will not be communicated. The second material used in this work is a composite made of the RPP matrix and a 20% of short recycled carbon fibers obtained by pyrolysis and then milled. The recycled fibers have a density of 1.8 g/cm^{-3}, a diameter of 7 μm and a nominal length of 180 μm. The composite plates were first elaborated by extrusion in order to obtain a homogeneous matrix-fibers compound and then by injection molding. As for the matrix plates, they were obtained only by injection molding. The elaboration process configurations are more detailed in Ref. 20.

Characterization

Film Purification. In the literature, some authors were able to identify IR peaks related to the phosphites that others could not.[22–25] So to better identify the peaks corresponding to the two antioxidants and to monitor their consumption during aging using FTIR and UV spectrophotometry, the phenol and phosphites were extracted for analyzing. The purification was performed on RPP and RPP-CF180 films having an average thickness of 25 μm and obtained by microtoming. The extraction procedure was carried out using a chloroform–ethanol–hexane (1:1:4) mixture under reflux for 48 h and then dried under vacuum at 40 °C.[21] After extraction operation, the residual sample was dried to obtain the pure stabilizer.

Infra-Red Spectrophotometry. FTIR spectrophotometry was performed in transmission mode on free standing films using a Frontier spectrophotometer (PerkinElmer). For each test, 32 scans were averaged in the 400 to 4000 cm^{-1} wavenumber

range to be able to obtain a 4 cm^{-1} resolution. The obtained spectra were analyzed using Spectrum software (PerkinElmer) in order to determine the absorbance value and therefor the concentrations of oxidant and antioxidant products by using Beer Lambert law:

$$A = \varepsilon_\lambda \cdot 1 \cdot C_\lambda$$

where A is the absorbance value, ε_λ (L mol^{-1} cm^{-1}) the molar absorptivity taken equal to $\varepsilon_{3646} = 117$ L mol^{-1} cm^{-1}, $\varepsilon_{1743} = 590$ L mol^{-1} cm^{-1}, $\varepsilon_{1718} = 350$ L mol^{-1} cm^{-1}, $\varepsilon_{768} = 440$ L mol^{-1} cm^{-1}, $\varepsilon_{887} = 318$ L mol^{-1} cm^{-1}, $\varepsilon_{1195} = 350$ L mol^{-1} cm^{-1}, $\varepsilon_{1234} = 250$ L mol^{-1} cm^{-1},[22–26] (Typical Infrared Absorption Frequencies) L (cm) is the film thickness and C_λ (mol L^{-1}) is he concentration of the considered species.

UV Spectrophotometry. Beside the IR spectrophotometry, UV analyzes were performed to follow the concentration evolution of the phenolic function. Since the concentration of phenolic stabilizer is very low (<1%), its value obtained by FTIR spectroscopy is not accurate. To do so, tests have been realized using a UV Perkin Elmer Lamba 35 Spectrophotometer.

Oxidation Induction Time Measurements. To characterize the presence of antioxidant in the matrix and composite, DSC tests under oxygen were performed in the aim of measuring the oxidation induction time (OIT). The experiments were realized on 4–7 mg mass samples heated from 50 to 200 °C at a heat rate of 10 °C min^{-1} under 1 bar of pure oxygen with a gas flow maintained at 50 mL/min.

Mechanical Characterization. Mechanical behavior of RPP and RPP-CF180 throw thermal aging was characterized under dynamic (high speed strain rate) and quasi-static loading. Dynamic tests were realized at 10 s^{-1} strain rate using a servo-hydraulic test machine (Schenck) equipped with a high speed camera (FASTCAM-APX RS) with the capacity of 250,000 frames per second to be able to record the pictures during high speed tensile test. The geometry of the specimen was optimized using ABAQUS finite element code in order to obtain a homogeneous strain distribution and a continued strain rate in the specimen's effective zone.[20] The quasi-static tests were performed at 10^{-2} s^{-1}, using INSTRON tensile-compression electromechanical device on specimen respecting ISO 527-2:1996 type 5A.

Exposure Conditions. Thermal aging under atmospheric air was carried out in ventilated oven at 120, 130, and 140 °C on matrix and composites films and specimens.

RESULTS AND DISCUSSION

FTIR Analysis

Figure 1 shows the infra-red spectrum of RPP matrix before and after purification. One can notice the presence of two peaks at 1743 and 3646 cm^{-1} related to the ester group and phenol function of the first antioxidant, respectively. Furthermore, four peaks related to the phosphites stabilizer are present: two medium at 768,876 cm^{-1}, a weak one at 1195 cm^{-1}[25] and a strong peak at 1234 cm^{-1} corresponding to the phosphonate (Typical Infrared Absorption Frequencies). The Ester absorption has a higher molar absorptivity than the phenol and does not
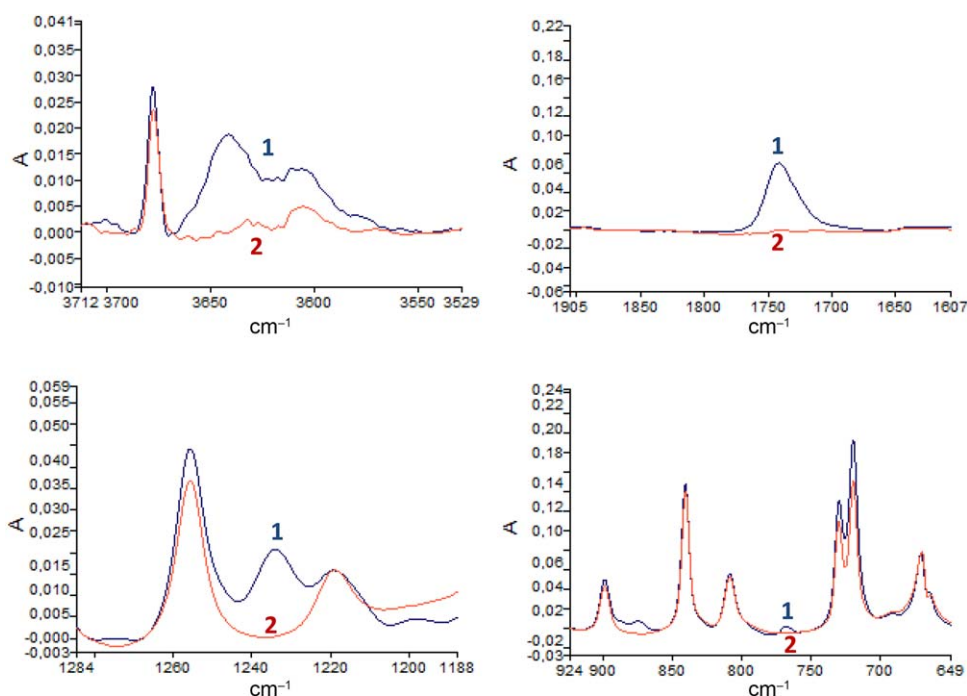
Figure 1. IR specter of RPP before (1) and after (2) stabilizer extraction. [Color figure can be viewed at wileyonlinelibrary.com]

interfere with the matrix absorption meantime OH signal does.[26] The same results were validated in the case of the composite.

OIT Measurements

Figure 2 shows measurement result of the OIT at 200 °C of the RPP matrix. It shows two endothermic peaks at 127 and 163 °C corresponding to the melting temperature of the polyethylene and polypropylene present in the blend respectively followed by a constant plateau due to the anti-oxidizing effect. After 343 min, an exothermic peak appears due to the oxidization of the material. It should be noted that a non-stabilized polypropylene that shows an average of OIT of 5 min.[27] A comparison between the OIT of the two materials is illustrated in Figure 3. This figure shows a lower OIT, about 331 min, for the composite compared to the pure matrix. This difference can be explained by a consumption of a part of the antioxidants during the extra extrusion process that the composite has undergone. This decrease of the antioxidant quantity will have a direct impact on the induction time.
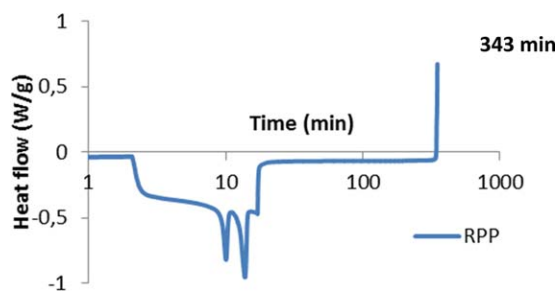
Carbonyl Build-Up and Stabilizers Disappearance

FTIR spectra evolution of the RPP matrix during exposure at 140 °C is shown in Figure 4. During exposure, the absorbance of ester peak (at 1742 cm^{-1}) decreases as another start to appear and increases at 1718 cm^{-1} which corresponds to the carbonyl build-up. The distinction between these different groups is not easy from a theoretical and experimental point of view. In fact, carbonyl and ester group are superposed in the same absorption peak. So, to be able to measure the real contribution of each group, a Gaussian deconvolution, using Origin Lab software was necessary. Once the spectrum deconvoluted, and by applying Beer Lambert law, mentioned above, the evolutions of ester and carbonyl groups are determined. Figure 5(a) compares the evolution of carbonyl group in the matrix and in the composite at 140 °C. One can note that the oxidation products appear and stabilize in the form of a plateau faster in the case of the composite. Thermal aging follow-up was stopped after 175 and 359 h for the composite and the matrix respectively. Since the ester group is not involved in the stabilization reactions, it is considered chemically stable. Thus, the evolution

Figure 2. Oxidation induction time (OIT) measurement for the RPP matrix. [Color figure can be viewed at wileyonlinelibrary.com]
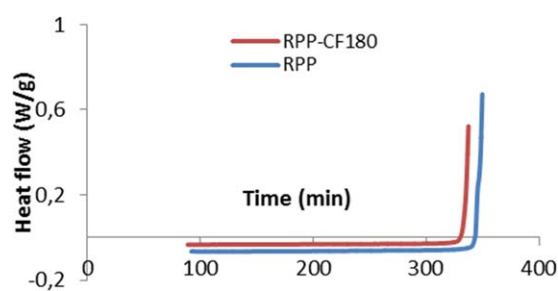

Figure 3. Comparison between OIT measurement for the matrix and the composite. [Color figure can be viewed at wileyonlinelibrary.com]
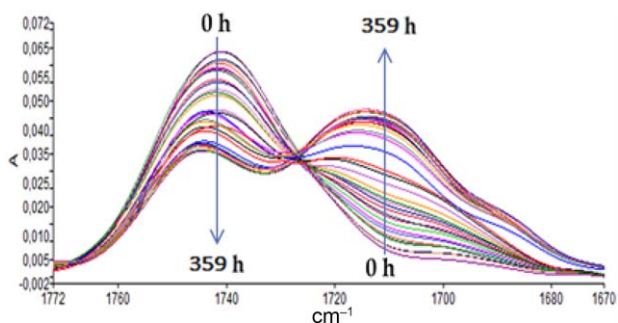
Figure 4. FTIR spectra of RPP matrix at 140 °C. [Color figure can be viewed at wileyonlinelibrary.com]

of its optical density will directly inform us about its physical loss, because of the evaporation.[24] Ester band starts to disappear from the very first moments of exposure and decays almost linearly as shown in Figure 5(b). It is obvious that the ester group in the composite decreases faster than RPP which affects the induction time and consequently the carbonyl build up rate. The maximum rate of the ester group loss (initial slope of the curves) is an increasing function of temperature. This rate are grouped in Table II for each exposure temperatures. As it can be seen, the ester groups disappear rapidly with the increase of exposure temperature. As for the evolution of the phenol concentration [Figure 5(c)], it shows a drop during the induction period followed by a plateau. Its evolution and concentration are different compared to literature. In fact, several works have shown that the phenol group disappears by chemical reaction and physical loss before the induction time is reached and its concentration value is much lower than the one shown in Figure 5(c).[15] Thus, one can suppose that another additive product is present at the same spectral range as the phenol; and its concentration does not change during the induction period. However, the results of the purification show previously in Figure 1 show that it is not possible to detect the presence of any other

product. Thus, the concentration evolution of this stabilizer will be realized through UV spectrometry and discussed in the following paragraph. Figure 5(d), represents the phosphites concentration decrease for the composite and the matrix. It shows that in one hand the initial concentration of this antioxidant is higher in the matrix than in the composite (0.0399 mol/L compared to 0.0375 mol/L) and in the other hand that this stabilizer is not totally consumed during the induction period but in the contrast, it disappears once the oxidation process stabilizes and it happens first in the case of the composite. It has been verified for each exposition temperature that the oxidation in the composite appears faster than in the matrix. Table I summarizes the induction time (t_i) for the two materials for each exposure temperature.

The UV spectrometry analysis of the two materials though aging at 140 °C is shown in Figure 6. The results show a wide UV absorption band consisting of two contributions between 250 and 300 nm related to the phenolic and phosphites antioxidants.

Since phosphites stabilizers have an aromatic group that contributes in the absorbance at 283 nm, it was not possible to determine exactly the contribution of phenol from the UV spectrum. To deal with this problem, the contribution of the phosphites aromatic group in the peak is subtracted. For that, the concentration of the latter is calculated thanks to IR spectrum and the UV contribution of phenol is given by the following equation:

$$[\text{Phenol}] = \frac{A_{283} - [\text{Phos}] \cdot \varepsilon_{\text{Ar}-\text{O}-\text{P}} \cdot l}{l \cdot \varepsilon_{\text{Ar}-\text{OH}}}$$

where A_{283} is the absorbance peak at 283 nm, [Phos] is the phosphites concentration measured by FTIR spectrometry, $\varepsilon_{\text{Ar}-\text{O}-\text{P}}$ (731 L mol^{-1} cm^{-1}) and $\varepsilon_{\text{Ar}-\text{OH}}$ (1439 L mol^{-1} cm^{-1}) are the molar absorptivity of phosphites and phenol at 283 nm, respectively.[28] By applying the precedent formula the initial concentration of phenol is slightly lower than that obtained by subtracting the plateau from the phenol curve in Figure 5(c). The kinetic curves of
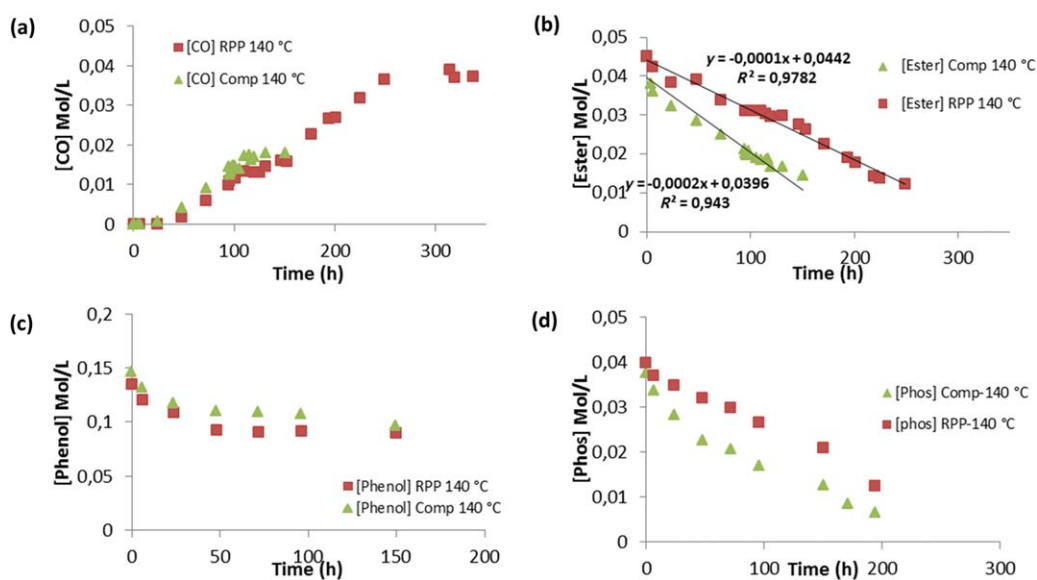

Figure 5. Comparison between kinetic curves for RPP and the composite at 140 °C: (a) carbonyl build-up, (b) ester group, (c) phenol, and (d) phosphites. [Color figure can be viewed at wileyonlinelibrary.com]

Temperature (°C) Induction time t_i (h)	120	130	140
RPP	175	60	42
RPP-CF180	95	36	24

Phenol concentration consumption of the matrix and composite at 140 °C are represented in Figure 7. Contrary to the results shown previously in Figure 5(c), these results show that the initial value of the concentration of phenols is in a concentration range similar to that found in the literature.[15] Moreover, the phenol concentration present in the matrix (0.0375 mol L^{-1}) is greater than that of the composite (0.0307 mol L^{-1}). In addition, these results show that the phenolic antioxidant is fully consumed before the induction time. Therefore, the shorter induction time in the case of the composite is explained by a lower initial concentration of the phenolic antioxidant.

Kinetic Model

A standard mechanism has been chosen considering both uni- and bimolecular hydroperoxide decomposition[29] and taking into account the antioxidants effect.[30–32] This mechanism is given by the following scheme:
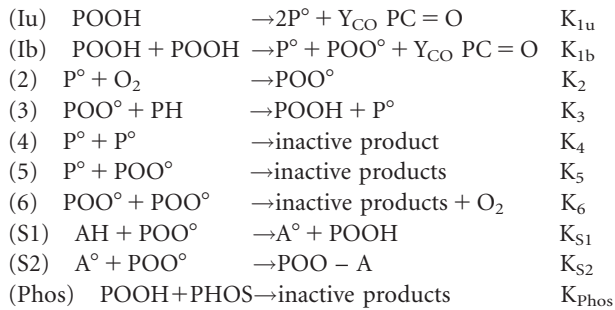
(Iu)	POOH	$\rightarrow 2P° + Y_{CO} \, PC = O$	K_{1u}
(Ib)	POOH + POOH	$\rightarrow P° + POO° + Y_{CO} \, PC = O$	K_{1b}
(2)	P° + O$_2$	$\rightarrow POO°$	K_2
(3)	POO° + PH	$\rightarrow POOH + P°$	K_3
(4)	P° + P°	$\rightarrow$ inactive product	K_4
(5)	P° + POO°	$\rightarrow$ inactive products	K_5
(6)	POO° + POO°	$\rightarrow$ inactive products + O$_2$	K_6
(S1)	AH + POO°	$\rightarrow A° + POOH$	K_{S1}
(S2)	A° + POO°	$\rightarrow POO − A$	K_{S2}
(Phos)	POOH+PHOS$\rightarrow$inactive products		K_{Phos}

Basing on these reactions, the following set of differential equations is derived:

$$\frac{d[P°]}{dt} = 2k_{1u}[POOH] + k_{1b}[POOH]^2 - k_2[P°][O_2] + k_3[POO°][PH] - 2k_4[P°]^2 - k_5[P°][POO°]$$
(1)

$$\frac{d[POO°]}{dt} = k_{1b}[POOH]^2 + k_2[P°][O_2] - k_3[POO°][PH] - k_5[P°][POO°] - 2k_6[POO°]^2 - k_{S1}[POO°][AH] - k_{s2}[POO°][A°]$$
(2)

$$\frac{d[POOH]}{dt} = -k_{1u}[POOH] - k_{1b}[POOH]^2 + k_3[POO°][PH] + k_{S1}[POO°][AH] - k_{PHOS}[POOH][PHOS]$$
(3)

$$\frac{d[PH]}{dt} = -k_{1u}[POOH] + k_3[POO°][PH]$$
(4)

$$\frac{\partial[AH]}{\partial t} = -k_{s1}[POO°][AH] - \delta_{AH}[AH]$$
(5)

$$\frac{d[A°]}{dt} = -k_{s1}[POO°][AH] - k_{S2}[POO°][A°] - \delta_{A°}[A°]$$
(6)

$$\frac{\partial[PHOS]}{\partial t} = -k_{PHOS}[POOH][PHOS] - \delta_{Phos}[PHOS]$$
(7)

where δ_{AH}, δ_{Phosh}, and $\delta_{A°}$ are the evaporation coefficients of phenol and phosphites and their radicals, respectively.

The system was solved numerically using Matlab Ode23s solver with the following boundaries conditions:

- At $t = 0$: [P°] = [POO°] = 0
- [POOH]$_0$ = 10^{-4} mol L^{-1}
- [PH] = 24 mol L^{-1}
- [O$_2$] = $S_{O_2} \times P_{O_2}$, S_{O_2} being the oxygen solubility in the matrix and P_{O_2} the external oxygen pressure of the atmosphere.
- [A°] = 0

The kinetic curves for the carbonyl build-up were generated using the following equation:

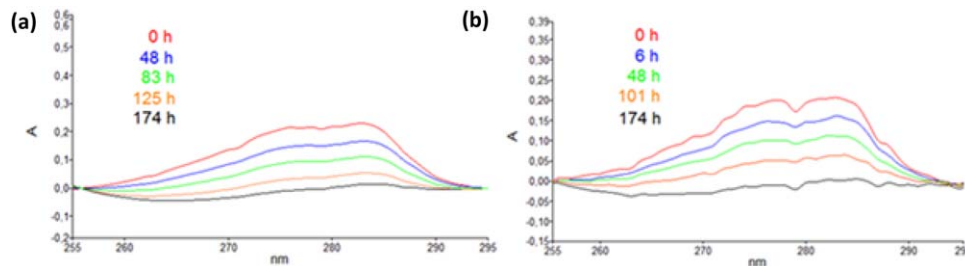| T (°C)	120		130		140	
	RPP	Composite	RPP	Composite	RPP	Composite
Dispersion rate of the ester groups (mol L^{-1} s^{-1})	-2×10^{-9}	-8.3×10^{-9}	-2×10^{-8}	-4.7×10^{-8}	-2.7×10^{-8}	-5.5×10^{-8}

Figure 6. UV spectra evolution of (a) RPP and (b) RPP-CF180. [Color figure can be viewed at wileyonlinelibrary.com]
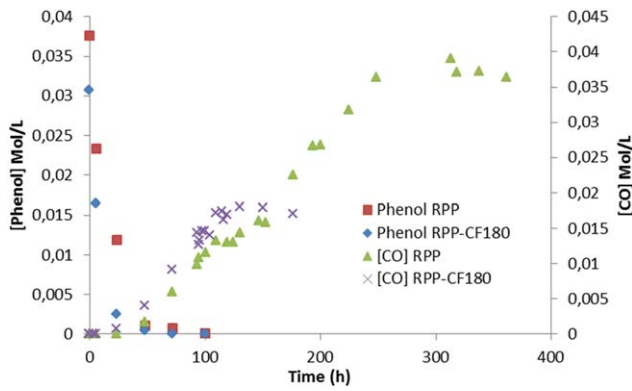
Figure 7. Phenol disappearance through oxidation of RPP and RPP-CF180. [Color figure can be viewed at wileyonlinelibrary.com]

$$\frac{d[PC=0]}{dt} = Y_{CO_u} k_{1u}[POOH] + Y_{CO_b} k_{1b}[POOH]^2$$

Y_{CO_u} and Y_{CO_b} are the carbonyl yields of the uni- and bimolecular POOH decomposition, respectively.[33]

Figure 8(a, b) show the different simulations of the carbonyl build-up and phenol extinction for the matrix and the composite at 140 °C. A good correlation between numerical kinetic curves and those obtained experimentally is clearly noticed. Figure 8(c) represents the numerical and experimental curves of phosphites concentration evolution for the two materials. The rate constants values that provided the best simulations of the experimental results corresponding to the different exposure temperatures are summarized in Table III. The orders of magnitude of the termination rate constants verify the relationship $K_4 \geq K_5 \gg K_6$ found in the literature.[34] The rate constants K_2, K_4, and K_5 involving a primary radical $P°$ which is very reactive, are independent of the temperature. This indicates that their activation energy is relatively zero. The value of k_3, responsible

for the carbonyl build-up rate, remains approximately the same for the matrix and the composite and increases with the increase of the temperature. The parameters k_{S1}, K_{S2}, and k_{Phos} responsible for the disappearance of the different antioxidants are changed. In fact, they increase as well with the increase of the temperature and are lower in the case of the composite since the oxidation occurs faster.

The determination of the model parameters for the tree exposure temperatures (Table III) allowed the calculation of the activation energy corresponding to each parameter. The different values of the activation energies are shown in Table IV. The activation energies values of the initiation and propagation steps calculated are realistic and similar to those found by Richaud et al.[19]

Influence of Thermal Oxidation on the Mechanical Behavior
The mechanical behavior of the matrix and composite was characterized through tensile tests at quasi-static (10^{-2} s^{-1}) and high strain rate loading (10 s^{-1}). The obtained stress/strain curves of the composite and the matrix specimens, taken at different times of aging at 140 °C, are represented in Figure 9. It is clear that the Young's modulus and the ultimate stress remain the same and are not affected by thermal aging but the elongation at break (E_r) is. Indeed, the elongation at break evolution at the quasi-static rate, illustrated in Figure 10, shows a dramatic drop by 40% and 45% for the RPP and RPP-CF180, respectively, from the very first moments of exposure to the induction time followed by a slow decrease until the end of the oxidation which is different from the results found in the literature. In fact Fayolle et al.[35,36] showed in their work on polypropylene, that the elongation at break is the most affected mechanical parameter by thermal aging. However, its evolution is characterized by a very small decrease during the induction period followed by a dramatic drop once the induction time is
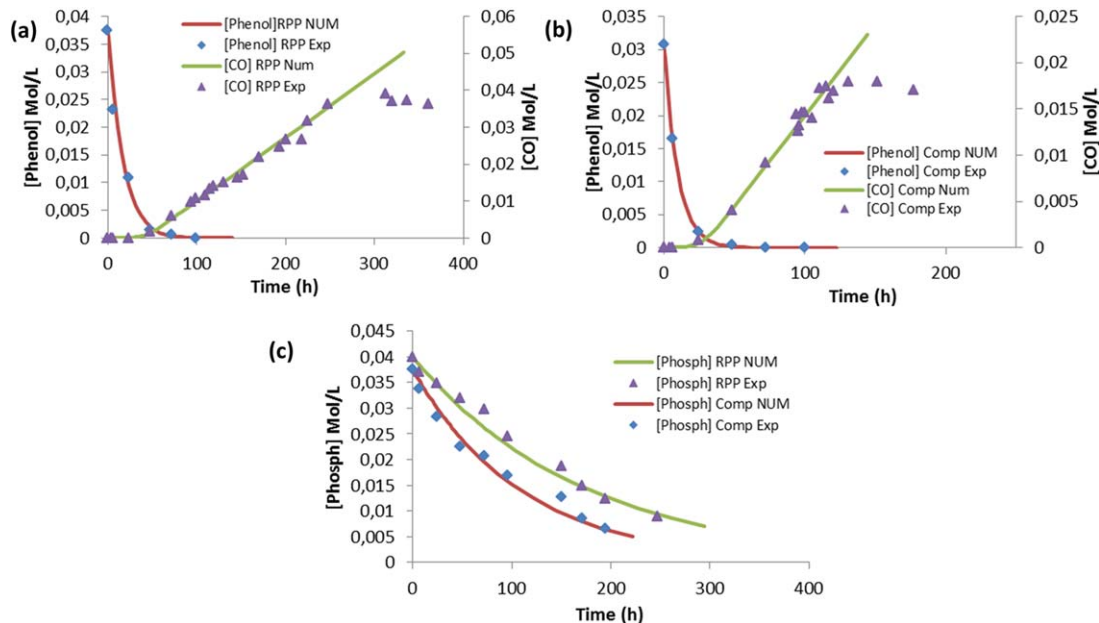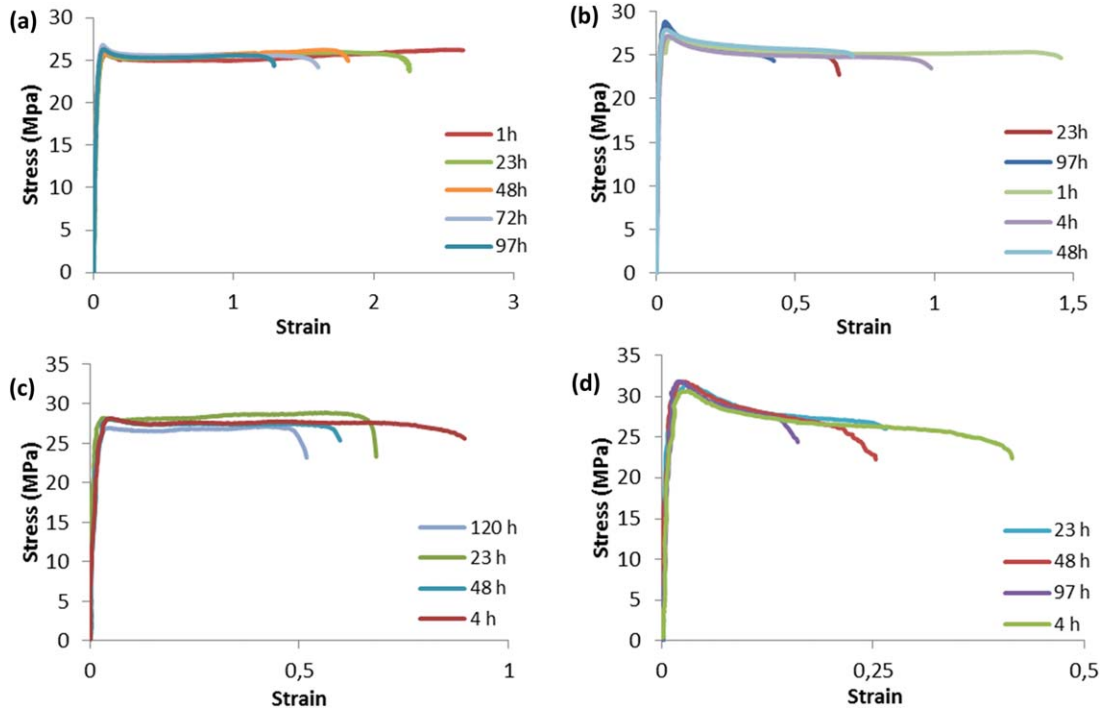

Figure 8. Numerical and experimental kinetic curves at 140 °C: carbonyl build-up and phenol consumption: (a) composite, (b) matrix (b) and (c) phosphites disappearance. [Color figure can be viewed at wileyonlinelibrary.com]

Table III. Kinetic Parameters of the RPP and RPP-CF180

Temperature (°C)	120		130		140	
Parameters	Matrix	Composite	Matrix	Composite	Matrix	Composite
K_{1u} (s^{-1})	2×10^{-6}	2.5×10^{-6}	7×10^{-6}	9×10^{-6}	10^{-5}	1.6×10^{-5}
K_{1b} (L mol^{-1} s^{-1})	2×10^{-3}	2×10^{-3}	8×10^{-3}	7×10^{-3}	10^{-2}	10^{-2}
K_2 (L mol^{-1} s^{-1})	10^7	10^7	10^7	10^7	10^7	10^7
K_3 (L mol^{-1} s^{-1})	0.011	0.012	0.019	0.02	0.026	0.027
K_4 (L mol^{-1} s^{-1})	2×10^9	2×10^9	2×10^9	2×10^9	2×10^9	2×10^9
K_5 (L mol^{-1} s^{-1})	10^8	10^8	10^8	10^8	10^8	10^8
K_6 (L mol^{-1} s^{-1})	1.4×10^6	2×10^6	2.1×10^6	2.5×10^6	2.9×10^6	3.1×10^6
K_{S1} (L mol^{-1} s^{-1})	0.12×10^2	0.1×10^2	0.22×10^2	0.14×10^2	0.3×10^2	0.2×10^2
K_{S2} (L mol^{-1} s^{-1})	1.25×10^{10}	1.2×10^{10}	1.35×10^{10}	1.3×10^{10}	1.5×10^{10}	1.4×10^{10}
K_{Phos} (L mol^{-1} s^{-1})	6×10^{-6}	5×10^{-6}	1.5×10^{-5}	1×10^{-5}	2.5×10^{-5}	2×10^{-5}
δ_{AH}	0.45×10^{-5}	0.7×10^{-5}	0.82×10^{-5}	1×10^{-5}	0.16×10^{-4}	0.28×10^{-4}
$\delta_{A°}$	10^{-3}	10^{-3}	10^{-3}	10^{-3}	10^{-3}	10^{-3}
B_{Phos}	0.4×10^{-6}	0.45×10^{-6}	0.8×10^{-6}	1.8×10^{-6}	1.6×10^{-6}	2.5×10^{-6}
Y_{COu}	1	1	1	1	1	1
Y_{COb}	1	1	1	1	1	1

Table IV. Activation Energies of the Two Materials

Parameters		K_{1u} (s^{-1})	K_{1b} (L mol^{-1} s^{-1})	K_2 (L mol^{-1} s^{-1})	K_3 (L mol^{-1} s^{-1})	K_4 (L mol^{-1} s^{-1})	K_5 (L mol^{-1} s^{-1})	K_6 (L mol^{-1} s^{-1})	K_{S1} (L mol^{-1} s^{-1})	K_{S2} (L mol^{-1} s^{-1})	K_{PHOS} (L mol^{-1} s^{-1})
Activation energy (KJ Mol^{-1})	RPP	109.101	108.71	0	54.836	0	0	51.554	61.99	12.28	96.27
	RPP-CF180	125.64	109.1	0	54.83	0	0	27.381	46.75	10.4	93.53

Figure 9. Stress–strain curves at quasi-static and dynamic loading: (a) RPP, (b) RPP-CF180 at 10 mm/min, (c) RPP, (d) RPP-CF180 at 10 s^{-1} for 140 °C. [Color figure can be viewed at wileyonlinelibrary.com]
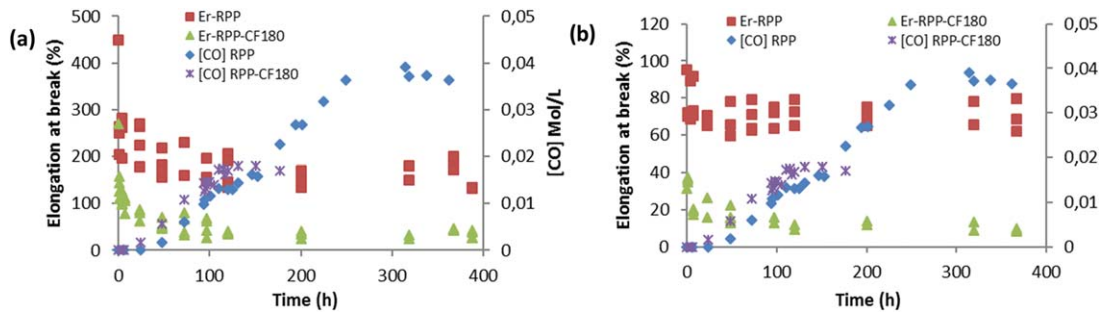
Figure 10. Elongation at break evolution at quasi-static and dynamic loading for 140 °C: (a) RPP and (b) RPP-CF180. [Color figure can be viewed at wileyonlinelibrary.com]

reached. In high strain rate loading, the two materials show a less important drop during the induction period, 25% and 34% for the matrix and the composite, respectively, but a same behavior of a small decrease till the end of oxidation. This phenomenon is due to the embrittlement of the matrix during exposure and to the weakening of the fiber/matrix interface in the case of the composite.

From an experimental point a view, during the induction period the carbonyl value is taken equal to zero because it remains too small and it is difficult to detect any changes. But in reality, it is not the case. In fact during this period, the polymer chains break to initiate the formation of radicals and then POOH responsible for carbonyl growth. In the case of the studied materials, the embrittlement occurs from the first moments of exposure during the induction period, so one can wonder what really happened during this duration. By taking a close look at

the induction period given by the model when the embrittlement at the quasi-static loading of the matrix and composite occurs, as represented in Figure 11, it is clear that the carbonyls start to appear but with a very small concentration that does not exceed 10^{-4} mol/L. Thus, it is possible not only to link the elongation at break with exposure time (Figure 10) but also with the quantity of [CO] present within the materials during the induction period as shown in Figure 12. As studied in the literature, the oxidation due to the penetration of oxygen in a thick exposed material occurs only at the surface, 100–200 μm, leading to an embrittlement and then final failure. In the case of the current study, the concentration of carbonyls formed at the beginning of exposure, even if it is too small considering their value after the induction time, participate in the embrittlement of the composite and the matrix causing a drop in the elongation at break. Hence, it is possible to couple the affected
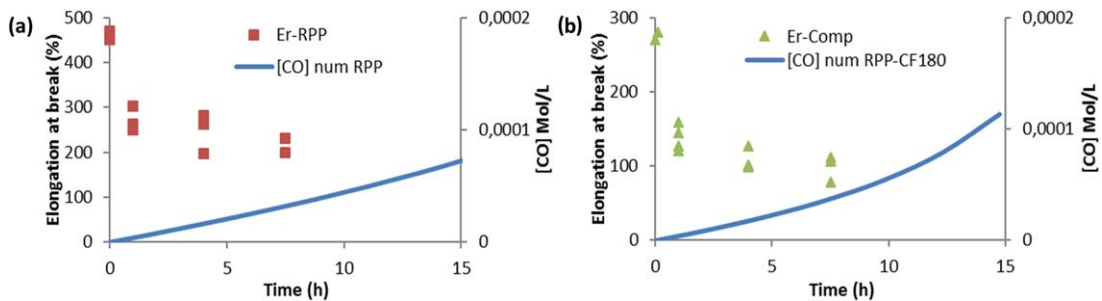

Figure 11. Comparison between elongation at break and numerical carbonyl growth at QS loading at 140 °C: (a) RPP and (b) RPP-CF180. [Color figure can be viewed at wileyonlinelibrary.com]
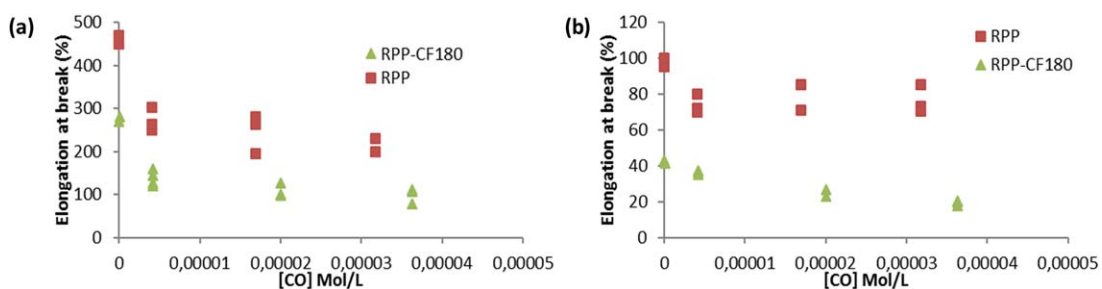

Figure 12. Elongation at break evolution Vs carbonyl build-up for RPP and RPP-CF180 at 140 °C: (a) Quasi-static, (b) Dynamic. [Color figure can be viewed at wileyonlinelibrary.com]

mechanical properties with a quantified parameter directly linked to the oxidation.

A direct relation between the oxidation products, [CO], and the elongation at break has been identified. Indeed, the oxidation is a surface phenomenon which affects on one hand the cracking of the matrix and on the other hand the fiber/matrix interface weakening. Thus, surface micro-cracking is favored and propagates into the material leading to failure. It has been shown that embrittlement of the surface by oxidation justifies the decrease of the elongation at break. Moreover, the results presented in this work make it possible to quantify this relationship. Further analyses dealing with the surface oxidative embrittlement phenomena will be the subject of a forthcoming publication.

CONCLUSIONS

In this article, the stabilization by phenol and phosphites of a new recycled blend and its reinforced carbon fibers composite has been studied during thermal oxidation at 140 °C. The induction time of the composite appeared to be shorter than that of the matrix due to a decrease in the concentration of the antioxidant during the extrusion and the injection molding processes. Several methods were used in the aim of determining the different evolutions of antioxidants concentration and carbonyl build-up through aging. A kinetic model which is based on a classic mechanistic scheme that takes into account in one hand uni- and bimolecular hydroperoxide decomposition and in the other hand the antioxidants effect was proposed and the elementary rate constants of the model were determined by inverse method. The obtained simulations of kinetic curves of carbonyl growth and the antioxidants' consumption showed a good correlation with those obtained experimentally with a reasonable physical loss. Thermal aging effect on the mechanical behavior of the studied materials was characterized under quasi-static and high strain loading. At both strain rates the overall mechanical behavior was not affected during thermal aging except for the strain at break which shows a decrease from the very first moment of exposure due to matrix embrittlement and fiber/matrix weakening. At low strain range, the drop of the elongation at break is higher than at high strain load. In fact, it is about 40% compared to 25% for the matrix and 45% compared to 34% in the case of the composite.

In further study, the obtained results will be coupled with damage investigation at a micro scale in order not only to characterize but also to quantify the damage initiation and kinetics during thermal aging at different temperature of exposure.

REFERENCES

1. Bos, G. EU Waste Legislation and the Composites Industry. Seminar on Recycling of Composite Materials, IFP SICOMP, Molndal, Sweden, 14th–15th May 2002.

2. Pickering, S. J. Compos. Part A 2006, 37, 1206.

3. Pimenta, S.; Pinho, S. T. Waste Manag. 2011, 31, 378.

4. Feih, S.; Mouritz, A. P.; Case, S. W. Compos. A: Appl. Sci. Manuf. 2015, 76, 255.

5. Yang, L.; Sáez, E. R.; Nagel, U.; Thomason, J. L. Compos. A: Appl. Sci. Manuf. 2015, 72, 167.

6. Sasse, F.; Emig, G. Chem. Eng. Technol. 1998, 21, 777.

7. Schwarzenbach, K.; Gilg, B.; Muller, D.; Knobloch, G.; Pauquet, J. R.; Rota-Graziosi, P. Plastics Additives Handbook, 5th ed.; Zweifel, H., Ed.; Hanser Gardner Publications: Cincinnati, OH, 2001.

8. Calvert, P. D.; Billingham, N. C. J. Appl. Polym. Sci. 1979, 24, 357.

9. Billingham, N. C. Plastics Additives Handbook, 5th ed.; Zweifel, H., Ed.; Hanser Gardner Publications: Cincinnati, OH, 2001; p 1019.

10. Ritter, A.; Michel, E.; Schmid, M.; Affolter, S. Polym. Test. 2005, 24, 498.

11. Bataillard, P.; Thomas, M. Plastics Additives Handbook, 5th ed.; Zweifel, H., Ed. Hanser Gardner Publications: Cincinnati, OH, 2001; p 1047.

12. Lundbäck, M.; Strandberg, C.; Albertsson, A.-C.; Hedenqvist, M. S.; Gedde, U. W. Polym. Degrad. Stabil. 2006, 91, 1071.

13. Strandberg, C.; Burman, L.; Albertsson, A.-C. Eur. Polym. J. 2006, 42, 1855.

14. Rosa, D. S.; Sarti, J.; Mei, L. H. I.; Filho, M. M.; Silveira, S. Polym. Test. 2000, 19, 523.

15. Richaud, E. Eur. Polym. J. 2013, 49, 2223.

16. Richaud, E.; Monchy-Leroy, C.; Colin, X.; Audouin, L.; Verdu, J. Polym. Degrad. Stabil. 2009, 94, 2004.

17. Bair, H. E. Polym. Eng. Sci. 1973, 13, 435.

18. Naskar, K.; Kokot, D.; Noordermeer, J. W. M. Polym. Degrad. Stabil. 2004, 85, 831.

19. Richaud, E.; Fayolle, B.; Verdu, J. Polym. Degrad. Stabil. 2011, 96, 1.

20. Meftah, H.; Tamboura, S.; Fitoussi, J. et al. Appl Compos Mater (2017). https://doi.org/10.1007/s10443-017-9632-6

21. Zahradníčková, A.; Sedlář, J.; Dastych, D. Polym. Degrad. Stabil. 1991, 32, 155.

22. Földes, E.; Maloschik, E.; Kriston, I.; Staniek, P.; Pukánszky, B. Polym. Degrad. Stabil. 2006, 91, 479.

23. Rugg, F. M.; Smith, J. J.; Bacon, R. C. J. Polym. Sci. 1954, 13, 535. Volume Issue

24. Lacoste, J.; Carlsson, D. J. J. Polym. Sci. Part A: Polym. Chem. 1992, 30, 493.

25. Djouani, F.; Richaud, E.; Fayolle, B.; Verdu, J. Polym. Degrad. Stabil. 2011, 96, 1349.

26. Djouani, F.; Patel, B.; Richaud, E.; Fayolle, B.; Verdu, J. Fuel 2012, 502.

27. de Lima, J. A.; Fitaroni, L. B.; Chiaretti, D. V. A.; Kaneko, M. L. Q. A.; Cruz, S. A. Chemistry 2017, 30, 504.

28. Vogel, P. Ecole Polytechnique Fédérale de Lausanne (EPFL), « Théorie « simpliste » de la couleur (spectroscopie UV-Visible) » 20.

29. Audouin, L.; Gueguen, V.; Tcharkhtchi, A.; Verdu, J. J. Polym. Sci. Part A: Polym. Chem. 1995, 33, 921.

30. Allen, N. S.; Chirinis-Padron, A.; Henman, T. J. *Polym. Degrad. Stabil.* **1985**, *13*, 31.

31. Pospíšil, J. *Polym. Degrad. Stabil.* **1991**, *34*, 85.

32. Pospíšil, J. *Polym. Degrad. Stabil.* **1993**, *39*, 103.

33. Richaud, E.; Farcas, F.; Fayolle, B.; Audouin, L.; Verdu, J. *Polym. Degrad. Stabil.* **2007**, *92*, 118e24.

34. Gillen, K. Y.; Wise, J.; Clough, R. *Polym. Degrad. Stabil.* **1995**, *47*, 149e61.

35. Fayolle, B.; Audouin, L.; Verdu, J. *Polym. Degrad. Stabil.* **2000**, *70*, 333.

36. Fayolle, B.; Audouin, L.; Verdu, J. *Polymer* **2004**, *45*, 4323.